Korean J. Chem. Eng., 35(5), 1174-1184 (2018)
DOI: 10.1007/s11814-017-0339-z

pISSN: 0256-1115
eISSN: 1975-7220

Thin film graphene oxide membrane: Challenges and gas separation potential

Fateme Abbasi*, Javad Karimi-Sabet,†, Cyrus Ghotbi*, and Zeinab Abbasi***

*Department of Petroleum and Chemical Engineering, Sharif University of Technology, Tehran, Iran
**Material and Nuclear Fuel Research School, Nuclear Science and Technology Research Institute, Tehran, Iran
(*Received 15 August 2017 • accepted 4 December 2017*)

Abstract−Graphene oxide membranes were prepared by vacuum and pressurized ultrafiltration methods on the 12% modified Polyacrylonitrile (12mPAN) substrate to specify challenges, salient features, future directions, and potential of GO membrane for separation fields using characterization techniques and gas separation test (studied gases are CO_2, He and N2), which is an efficient tool for better understanding of GO membrane behavior. GO membrane structure was examined over a wide range of parameters, such as pore size range of substrate and its surface properties, pH of GO dispersion, GO content, synthesis pressure, operating pressure and temperature. The results show that the GO content does not hold a linear relationship with the permeance and selectivity. Film thickness, aggregates, synthesis pressure defects and interlayer spacing have significant effects on the gas separation performance of GO membranes which originate from the synthesis method and its conditions.

Keywords: Aggregate, Defect, Graphene Oxide, Membrane, Interlayer Spacing, Gas Separation

INTRODUCTION

Graphene and graphene oxide (GO) have attracted much attention due to their broad spectrum of applications. GO has been used as a property enhancer, multifunctional crosslinker in thermosets [1], removing of nickel (Ni(II)) from aqueous solutions [2] and superior adsorbents for the removal of Pb(II) ions from aqueous solutions [3]. Photocatalytic applications of GO have been shown by Nguyen-Phan et al. [4] and Sen et al. [5]. Graphene oxide is an interesting material since the oxygen groups can be replaced by other functional groups according to the intended application. Separation applications are relatively new topics among the broad applications of graphene oxide because of the rigid structure of graphene oxide nanosheets that are impermeable to all molecules. Graphene oxide has been used for reverse osmosis because it is permeable to water but impermeable to most other substances [6-9]. GO membrane is a barrier to very small molecules such as helium under the humid conditions, whereas CO_2 can penetrate easily through it. When GO film is immersed in water, allowing some solutes with hydrated radii larger than 4.5 angstroms to pass through it [10,11]. GO is useful for desalination [12-14] and dehydration [15] because of its high hydrophilicity. Kim et al. focused on the gas-transport properties of thin film graphene and GO membranes [16]. They achieved high carbon dioxide/nitrogen selectivity by well-interlocked GO membranes synthesized by spin coating, under humid conditions. Although GO thin film membrane has had good performance in separation field [6,10,11,13,15-20], the presented results of some research are inconsistent. For example, Hang et al. reported selectivity as high as 3400 and 900 for H_2/CO_2 and H_2/N_2 mixtures, respectively, through selective structural defects on GO membrane synthesized by vacuum filtration [17] while Kim et al. [16] reported much less selectivity.

A review of the literature suggests that the effects of contracting synthesis and operating parameters on the GO thin film structure are not investigated simultaneously. To achieve the GO thin film membrane with good separation performance, many parameters are involved. In this work, to identify the effect of these parameters, GO thin film membrane was fabricated by pressurized and vacuum filtration method, and GO thin film structure was studied in a various range of parameters by characterization techniques and gas separation test (studied gases were N_2, He, CO_2). The most of these effective factors/parameters are as follows: material and pore size range of substrate, amount of GO used in filtration per unit membrane area (GO content: 0.003 $mgcm^{-2}$ to 1.556 $mgcm^{-2}$), synthesis pressure (p_{syn}: 15, 10, 6 and 2 bar and under vacuum condition), pH of GO dispersions used in filtration (pH: 2, 3.7, 6, and 10), operating pressure (p_{opt} 0.083 to 2 bar) and operating temperature, which are pressure and temperature applied during gas separation, respectively.

The main objective of this work was not to investigate gas separation performance of GO membrane or to introduce a membrane with high selectivity since it is well known that high performance of GO membranes in aqueous solutions mainly results from the unique water transport properties [21], but to specify the parameters that improve or decrease the membrane performance, demonstrate the salient features and challenges of thin film GO membranes for separation fields, and evaluate the potential of GO membrane for gas separation. Gas separation test is an efficient tool to identify the effective parameters and available challenges, while it is impracticable to attain detailed information on the GO film structure in the area of interest by characterization techniques. Therefore, the gas separation test along with the characterization techniques helps

†To whom correspondence should be addressed.
E-mail: j_karimi@alum.sharif.edu, jvkarimi@aeoi.org.ir

us to find a more reliable membrane structure, and the results are useful for all separation fields.

MATERIAL AND METHOD

Aqueous GO dispersions at various concentrations and pHs (pH: 2, 3.7, 6, and 10) were loaded in the static cell and filtered by the 12% modified Polyacrylonitrile ultrafiltration (12mPAN) substrate under vacuum and feed pressures of 2, 6, 10 and 15 bar. To evaluate the effects of microfiltration substrates, commercial polyamide microfiltration membrane with an average pore size of 450 nm was used as the microfiltration substrate. Pure gas (He, N_2, CO_2) permeation measurements of the GO membranes were performed using a constant-volume variable pressure method. The reader is referred to supporting information (see part 1 and 2.1 to 2.2) for details on the experiments and characterization of graphite oxide and GO dispersion.

RESULTS AND DISCUSSION

The membranes are denoted by an x-y membrane, representing the GO content ($mgcm^{-2}$) x and synthesis pressure (bar) y. All gas permeance tests were performed more than three times. Run to run reproducibility and sample to sample reproducibility were high and relative errors from the mean values of permeance were within ±1% and ±5%, respectively. Note that N_2, He and CO_2 indicate the permeance (GPU) of nitrogen, helium, and carbon dioxide gases, while SHe/CO_2 and SHe/N_2 represent the selectivity of corresponding gases.

1. Effect of Substrate

One of the most important parameters is the synthesis of desired substrates. The desired substrate should have two principal properties: 1) driving force required for the passage of water through the membrane should be provided at low synthesis pressures, and 2) the average pore size of the substrate should be smaller than GO flakes with narrow pore size distribution. Fig. 1 shows 0.14 $mgcm^{-2}$ GO membranes synthesized on the polyamide substrate (GO/PA) as microfiltration substrate and on the 12 wt% modified Polyacrylonitrile as ultrafiltration substrate (12mPAN, see section 2.3 of supporting information for a detailed discussion about this substrate). Mean pore size of polyamide membrane is 450 nm, while mean pore size and roughness of 12mPAN are 30 nm and 6.5 nm, respectively (see section 2.4 of supporting information). As shown in this figure, the perfectly uniform surface of GO is seen on the polyamide, but its permeance is almost similar to the substrate (Polyamide) permeance; the reason for this is obvious from its SEM image in Fig. 1. The surface of GO-PA membrane is non-uniform and porous, while the GO film formed on the PAN substrate has a dense structure for the same GO content. Therefore, to achieve almost the same permeance in both substrates, more GO amount is required for the case of PA substrate, which causes less selectivity, greater fragility, and more unevenness than PAN one. Therefore, 12 wt% modified Polyacrylonitrile substrate (12mPAN) is the best substrate as discussed in supporting information (see

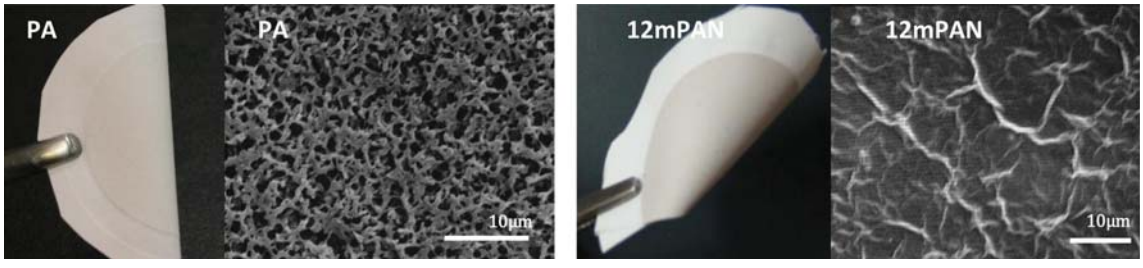

Fig. 1. GO membrane (p_{syn}=2 bar and GO content=0.14 mg/cm^2) supported on porous polyamide (PA) and 12mPAN.

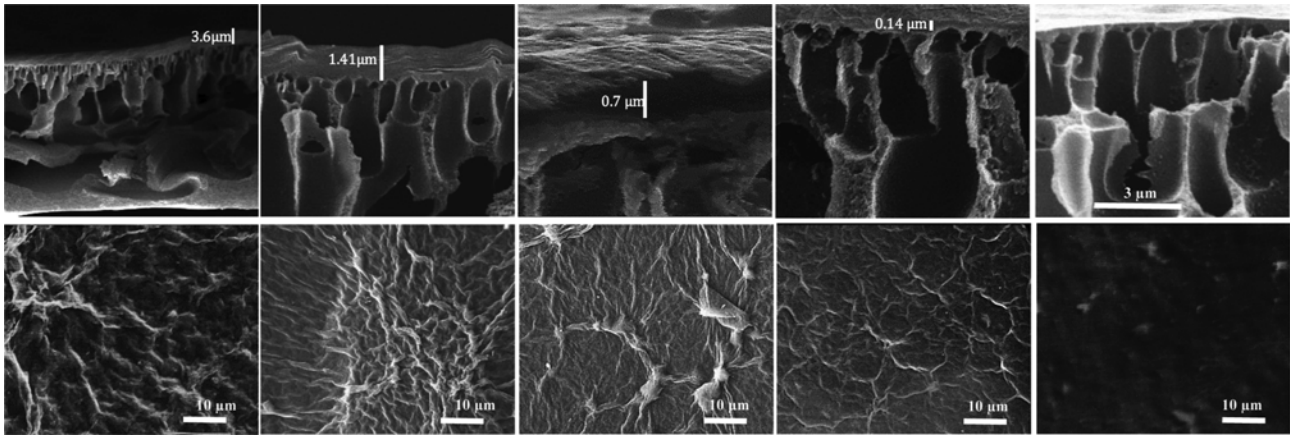

Fig. 2. SEM images of surface (low row) and cross section of GO membrane synthesized at p_{syn}=10 bar at various GO contents (from left to right: 0.707, 0.28, 0.14, 0.028 , 0.004 mg/cm^2).

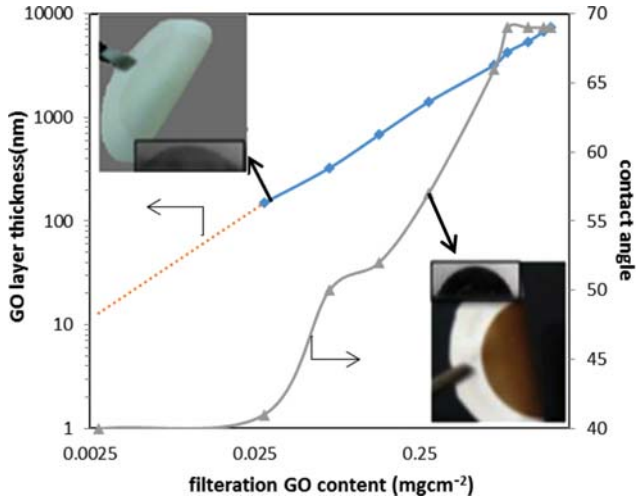

Fig. 3. Effect of GO content on GO film thickness and the contact angle of GO membrane synthesized at 10 bar pressure.

part 2.3 of supporting information).

2. Effect of GO Content

Fig. 2 and Fig. 3 indicate that the GO film thickness is linearly proportional to GO content; moreover, GO content affects the surface roughness as clearly depicted in Fig. 3. This fact is also realized by contact angle in Fig. 3 showing that the higher roughness results in the higher contact angle and by AFM images where average roughness increases from ~12 nm to ~154 nm when GO content increases from 0.028 to 1.56 mg/cm^2 (see part 2.4 of supporting information). SEM images (Fig. 2) were used to examine the surface and cross-morphological features of graphene oxide/12mPAN membrane (GO membrane) with an emphasis on the layer thickness and good attachment of GO layer to 12mPAN substrate through hydrogen bonds. The dense assembly structure of GO film, lamellar structure, the effect of GO content on the surface and cross-section of the GO/12mPAN membrane can be clearly seen in Fig. 2. The lamellar structure of GO membrane has been reported by other authors [16,18,22]. Furthermore, the good attachment between

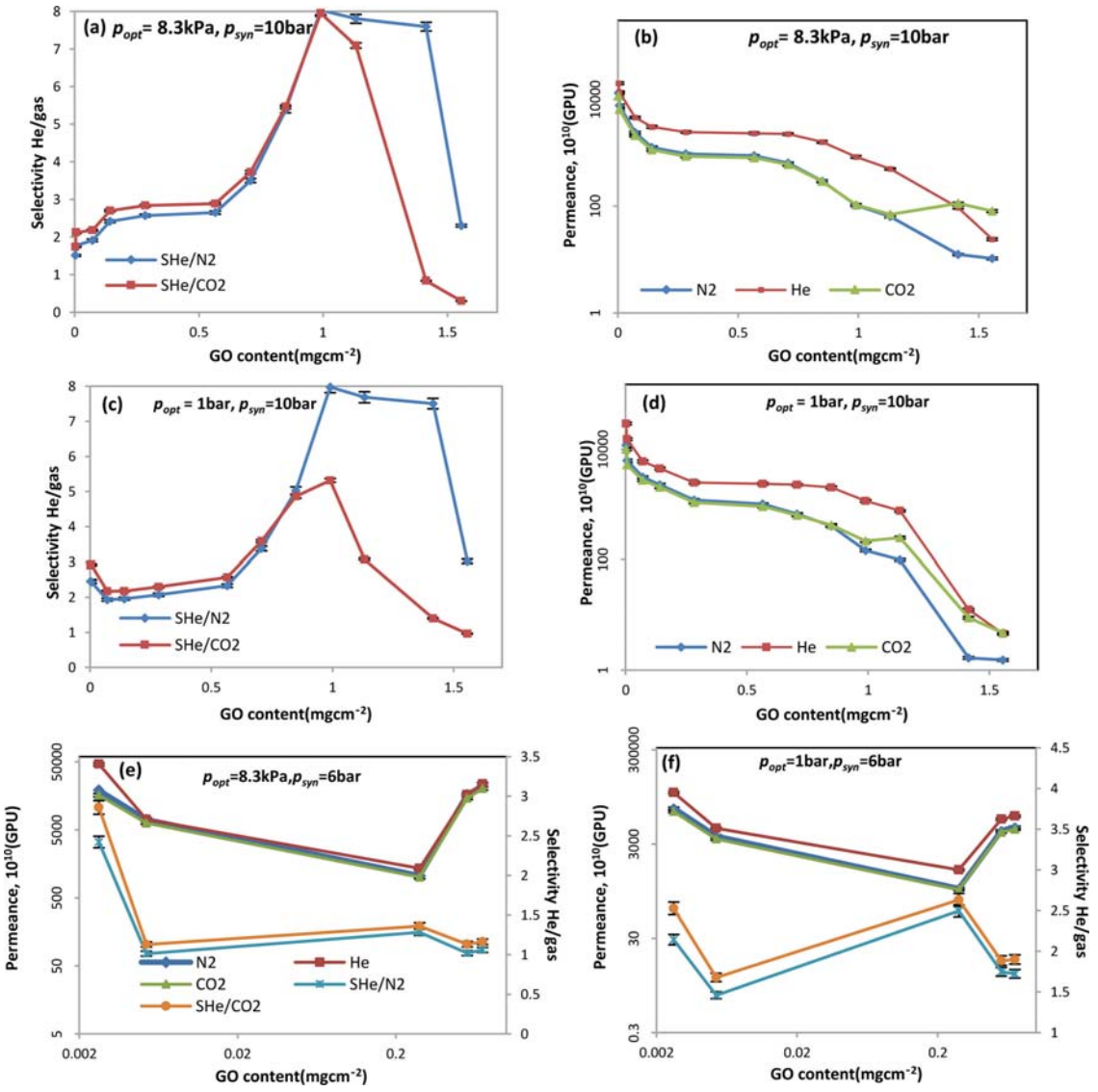

Fig. 4. Permeance and selectivity of GO membranes at various GO content and synthesis pressure at p_{opt}=8.3 kPa and 1 bar.

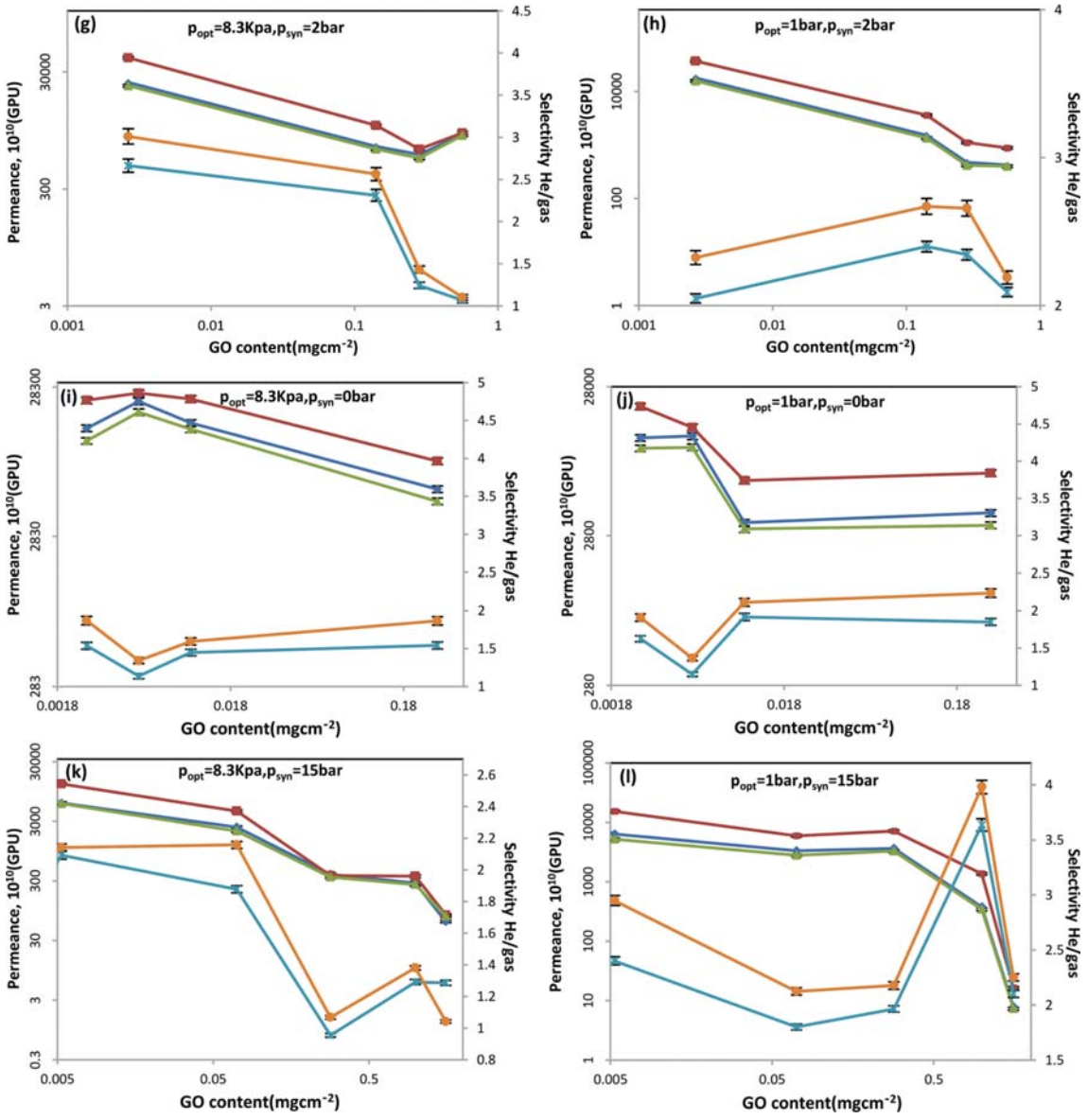

Fig. 4. Continued.

-COOH or -$CONH_2$ groups of the 12mPAN substrate and the GO hydroxyl and carboxyl groups was achieved through hydrogen bonding interactions and no peeling off occurs. The hydrogen bonds and residual π-π interaction hold the GO layers together and result in the laminate structure of GO film [23].

3. Effect of GO Content, Synthesis, and Operating Pressure

The effect of GO content is indicated in the Figs. 4(a) to 4(d). To explain the effect of various contracting parameters, the range of GO content was divided into several subranges. Furthermore, for a better understanding of membrane performance in each subrange, the reader is referred to the other figures. The permeation results show that the GO content does not hold a linear relationship with the permeance and selectivity of He/N_2 mixture (Fig. 4). At very low filtration GO content (about 0.00149 mgcm^{-2}), it is difficult to reach complete coating of graphene oxide on the substrate surface. According to permeation results, no selectivity enhancement can be obtained under these conditions. Although a dense smooth surface can be formed at GO content of 0.004 to 0.07 mgcm^{-2} (Fig. 2), relatively low selectivity will be obtained due to few nanometer thick film of GO deposition. The low He/N_2 selectivity of ~1.8 was reported by Kim et al. [16] for the low thickness of GO film prepared by spin coating. In such amounts of graphene oxide, the permeance of GO membrane synthesized at 10 and 15 bar is less than that of 6, 2 bar and vacuum (see Figs. 4 to 8) because the resistance of the nanochannel against gas transport is weakened with the enlargement of interlayer spacing due to the lower synthesis pressure, and consequently lower selectivity can be achieved.

The XRD is employed to reveal the effect of pressure on the interlayer spacing of GO film. The peak of GO film is around 23 degree, which is found by comparing the XRD spectrum of the GO-membrane and its sublayer. GO film peak shifts to the larger ones with an increase in the synthesis pressure as shown in the

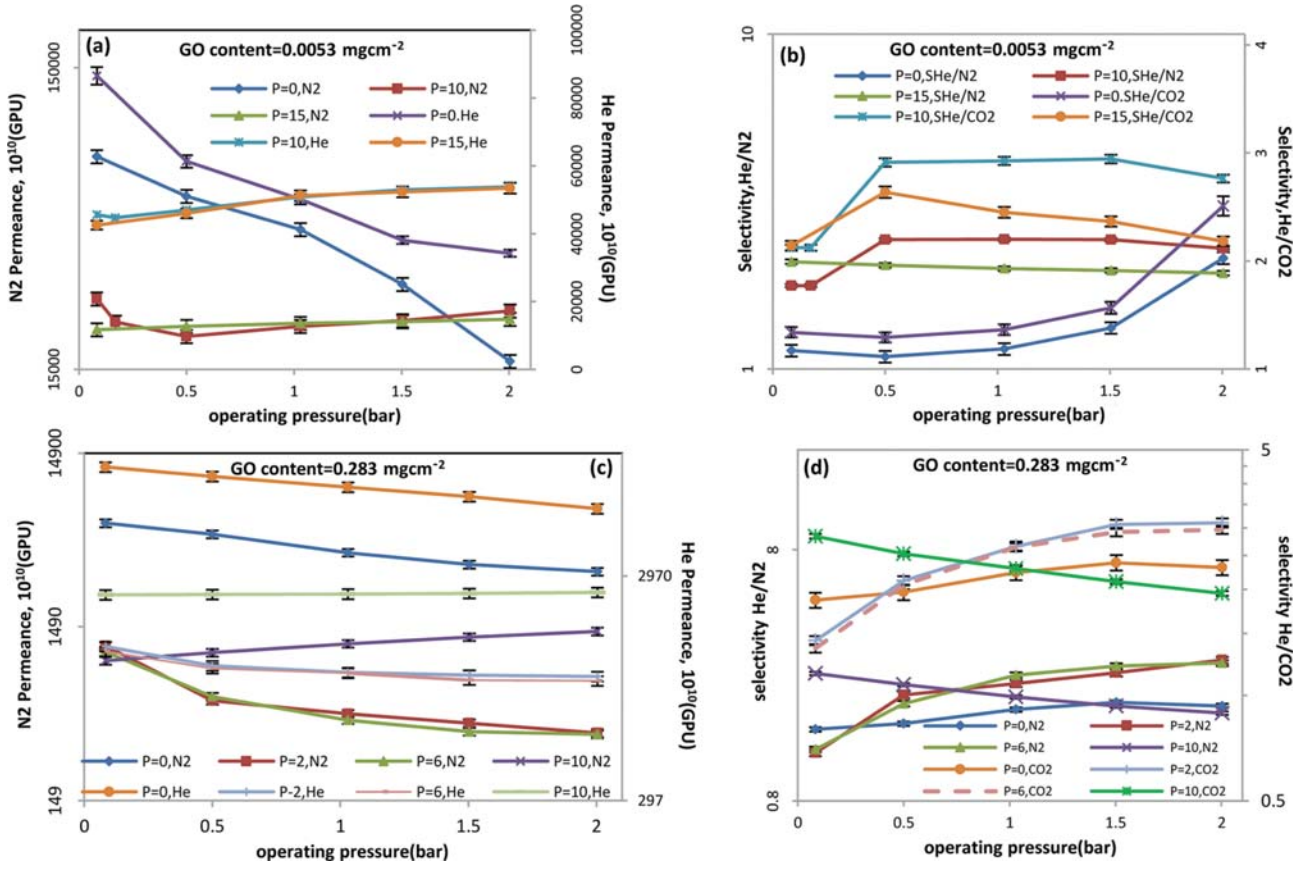

Fig. 5. Effect of operating pressure on permeance at various synthesis pressures for 0.283 mg/cm^2 and 0.0053 mg/cm^2 GO membranes.

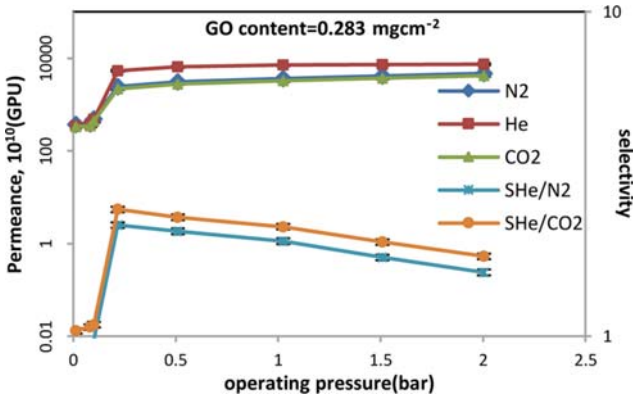

Fig. 6. Effect of operating pressure on permeance at synthesis pressure of 15 bar for 0.283 mg/cm^2 GO membrane.

Fig. 9(a). In fact, the interlayer spacing is inversely proportional to synthesis pressure. According to Fig. 9(b), the film density and surface roughness of GO membrane increase with GO content (due to longer synthesis time) and synthesis pressure. In this range of GO content, the permeance of x-y (2,6 and vacuum) membrane is inversely proportional to the operating pressure, while permeance of x -15 membrane increases with operating pressure, whereas x -10 membrane experiences a different trend dependent on GO content (see Figs. 5 to 8).

The upward trend of the permeance with operating pressure implies that the film may undergo a physical process, which is common in the gas separation by the polymeric and ceramics membranes [24], whereas permeance reduction with the operating pressure is contrary to what is reported in the literature for ceramic and polymeric membranes, but this trend is expected in the GO membranes due to the lamellar structure of these membranes. Operating pressure affects the gas permeance in two ways: 1) similar to polymeric and ceramic membranes, the permeance increases due to conventional mechanisms, such as solution diffusion, surface diffusion, etc. [25]. In addition, the kinetic energy of gases increases with operating pressure to overcome energy barrier of cavities [16] and this causes higher permeance at higher operating pressure. 2) The gas permeation rate through the GO film decreases due to increase in the film density, which arises from higher tortuosity coefficient and blocking some paths of gas passage (see Fig. 10). The effect of operating pressure is more pronounced for the membranes synthesized at low pressure. In fact, GO membrane undergoes a physical change in structure with changing synthesis pressure through film density and pressure defects; consequently, this directly affects the membrane performance. At lower synthesis pressures, the film density of the GO membranes decreases and more distance between GO flakes is observed. The arrangement of GO flakes also changes with operating pressure. GO flakes tend to become closer together with an increase in operating pressure, which causes some available paths for gas transport trough GO film to

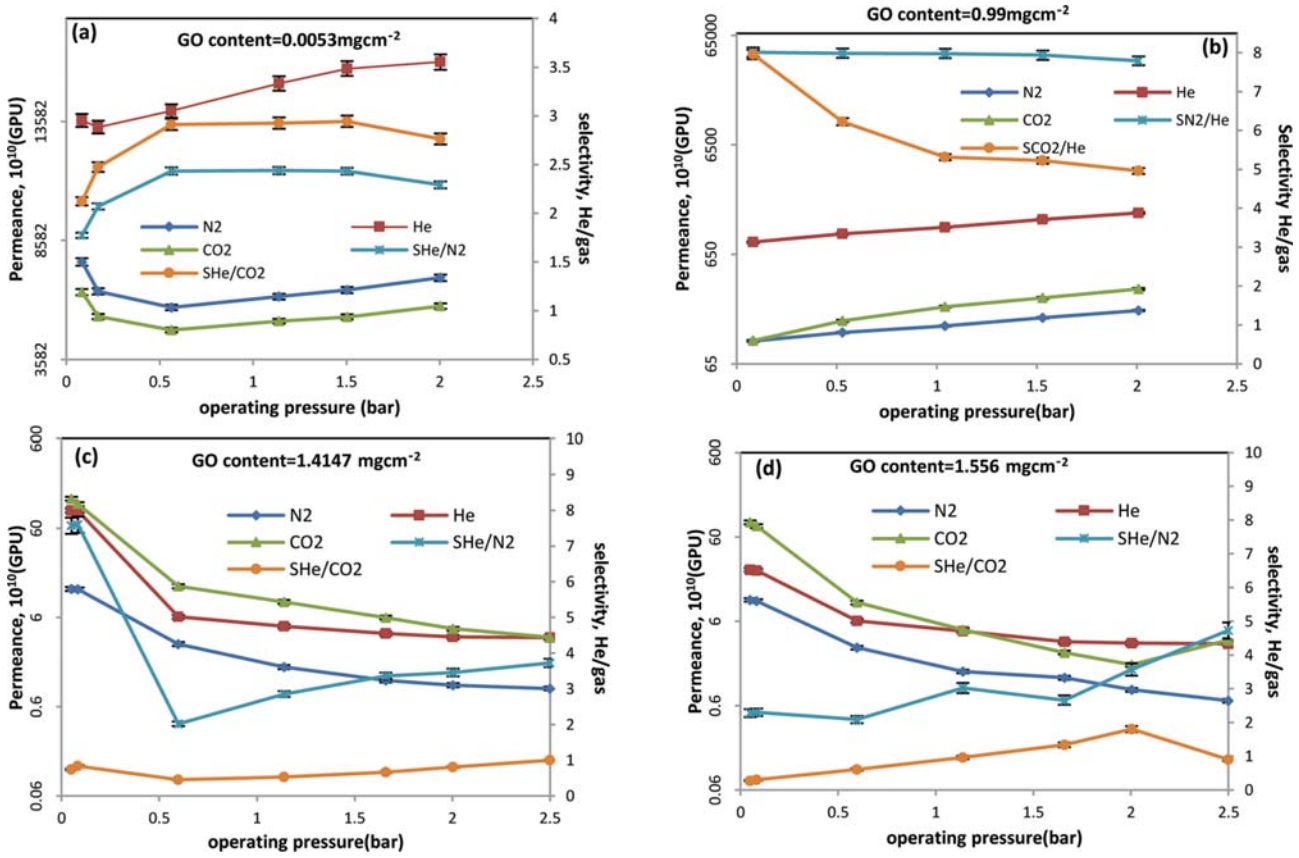

Fig. 7. Effect of operating pressure on permeance and selectivity at synthesis pressure of 10 bar for various GO contents.

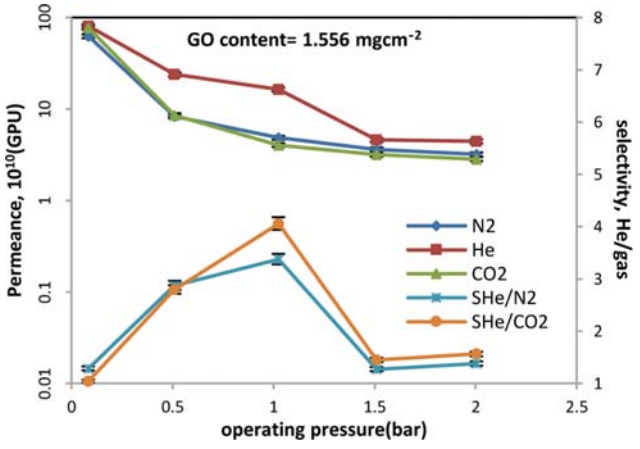

Fig. 8. Effect of operating pressure on permeance and selectivity at synthesis pressure of 15 bar for 1.556 mg/cm^2 GO membrane.

be blocked. As a result, tortuosity factor and the resistance to the passage of gas obviously increase and finally, the effective cross section for gas transport becomes smaller. This change in GO film structure with operating pressure always competes with an increase in kinetic energy. When the former factor becomes dominant, permeation decreases with operating pressure. For example, He permeance of 0.0053 GO membrane decreases to 60% when operating pressure increases from 8.3 kPa to 1bar (see Fig. 5).

No symptom of operating pressure remains in the membrane structure after removing the operating pressure (see part 2.5 in supporting information for more explanation). The dense layer thickness increases from 0.33 to 2.7 μm as GO content changes from 0.07 to 0.57 (Fig. 3); when this happens, the resistance to the passage of gas obviously increases, but this enhancement is not proportional to the rise in GO content (see Figs. 4(a) to 4(d)). This trend may be attributed to structural defects in the GO film during filtration due to pressure stress and high filtration time at such high GO content because first-coated GO layers cannot withstand high-pressure stress. These structural defects make nonselective paths for passage of gas through the GO membrane, and consequently the permeance increases. However, the resistance rise is somewhat at odds with this effect; thus the permeance slightly decreases when the GO content increases further (i.e., from 0.07 to 0.57 mgcm^{-2}). This effect is more dominant at higher synthesis pressure and higher GO contents. For example, the permeance of 1.5556-15 membrane is greater than 1.5556-10 one in both operating pressure of 1bar and 0.083bar; and the permeance of 0.2839-15 membrane is greater than 0.2839-10 one in the operating pressure of 1 bar (Figs. 4(c) and 4(l)); these confirm that despite the more film density at higher synthesis pressure, the permeance increases due to increase in these structural defects. For GO content from 0.07 to 0.7 mgcm^{-2}, the membranes synthesized at a pressure of less than 10 bar experience a different permeance trend from those synthesized at a pressure of 10 bar. These membranes have

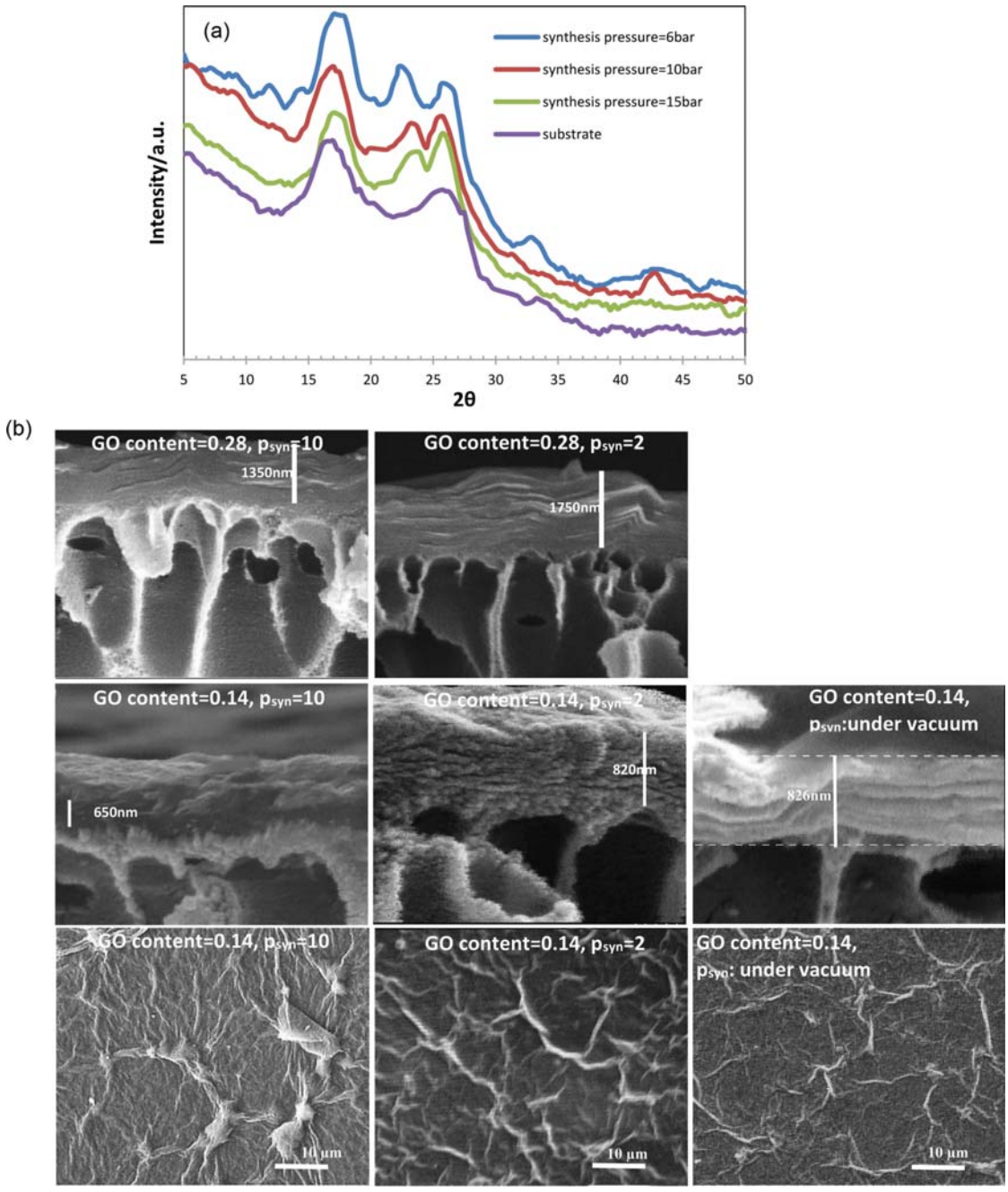

Fig. 9. Effect of synthesis pressure on (a) interlayer spacing of substrate and GO membranes and (b) cross section of 0.28 mg/cm^2 GO membrane (upper row), cross-section (middle row) and surface (lower row) of 0.14 mg/cm^2 GO membrane. Left to right: p_{syn}=10, 2 bar and under vacuum.

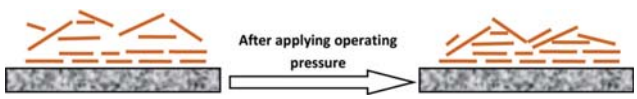

Fig. 10. Effect of operating pressure on interlayer spacing.

lower selectivity, which decreases with further increase in the GO content (Figs. 4(a) to 4(j) and 5). Therefore, synthesis of thicker GO membranes at such low pressure is not reasonable.

GO membrane thickness is approximately doubled with doubling GO content from 0.28394-x to 0.565888-x (x=2, 6 bar) mgcm^{-2} (Fig. 3); when this happens, it is expected that the permeance considerably decreases, but according to Figs. 4(e) to 4(h), the permeance has been increased. One reason for increasing permeance is the synthesis pressure defects especially at such high GO content, but this cannot be the only reason for the increase in the permeance since despite the more pressure defects for the same membrane synthesized at 10 bar, no increase in the permeance occurs. It seems that there is another influential factor; this factor is the formation of layers on top of the membrane by the aggregates

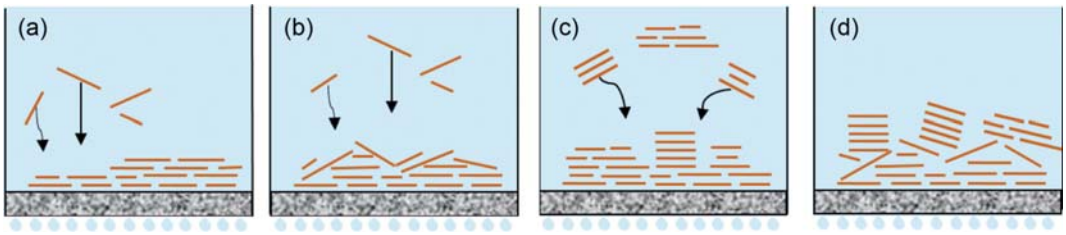

Fig. 11. Possible structures of GO film.

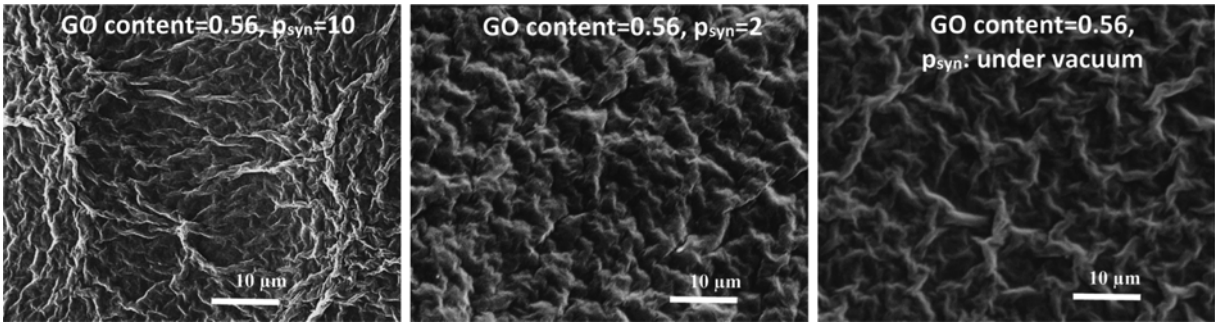

Fig. 12. Aggregates at various synthesis pressures for GO content of 0.56 mg/cm^2. Left to right: 10 bar, 2 bar, and under vacuum.

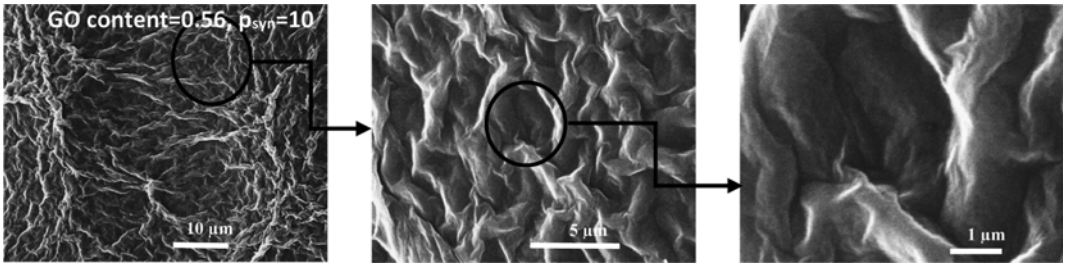

Fig. 13. The surface of GO membrane with GO content of 0.56 mg/cm^2 and p_{syn}=10 bar.

(Fig. 11), which is implied by SEM images of GO membrane surface (see Figs. 12 and 13). The GO dispersion tends to become more concentrated with the withdrawal of water during filtration, leading to unstable GO dispersion that is revealed by aggregates; these aggregates make the building blocks of top layers of GO membrane. This problem is most commonly seen at higher GO content and lower synthesis pressure because the synthesis takes longer, and consequently the opportunity for aggregate formation increases. In fact, the single layer GO flakes do not make the building blocks of the membrane and the possibility of formation of structure A and even structure B is very low during filtration, especially at high GO content. The structure B may be observed at low GO content and high synthesis pressure, and the structure B with less interlock can be achieved at low synthesis pressure or under vacuum condition (Fig. 10). Graphene oxide films are built from aggregates with various sizes so that larger aggregates form the upper layers and the first layers may be formed by single layer GO flakes (see Fig. 11(d) and (c) structure). The resistance of the channels against gas transport is weakened due to the presence of the aggregates in GO film. This factor along with the other factors cause the permeance to be less than the expected one, and in some cases, such as the case was introduced, the permeance increases.

According to the above explanation, the effect of interlayer spacing, GO film thickness, pressure stresses, structural defects and aggregates in the top layers on the permeance and selectivity of the GO membrane should be considered simultaneously. By comparing permeance data of membranes synthesized at pressures 10 and 15 bar (see Figs. 4(a) to 4(d) and 4(k) to 4(l)) can be found that despite higher film density at higher synthesis pressure, the performance of membrane synthesized at 10 bar is better than the same one synthesized at 15 bar due to more pressure defects at high synthesis pressure; therefore, the best synthesis pressure is equal to 10 bar. The selectivity of helium to nitrogen enhances from 2.6 to 8 with an increase in GO content from 0.7 mgcm^{-2} to 0.99 mgcm^{-2}, as shown in Figs. 4(a) to 4(d). The maximum selectivity of He/N_2 and He/CO_2 occur at GO content of 0.99 mgcm^{-2}. For this membrane, synthesis pressure and GO content act in a manner that selective channels for the passage of gas through GO film are created. By increasing the GO content from 0.99 mgcm^{-2} to 1.56 mgcm^{-2}, both permeance and He/N_2 selectivity are dropped. Moreover, the film structure is so dense and interconnected at such high GO content that the passage of gas will be difficult for both nitrogen

and helium. The increase in resistance is at odds with other effects; thus the permeance decreases. Selectivity reduction can be attributed to pressure defects and more aggregates which create non-selective nanochannels. Thus, GO dispersion tends to become more concentrated during filtration with an increase in GO content from 0.99 to 1.56, leading to formation of more aggregates. These aggregates deposit and make the building blocks of GO membrane. On the other hand, filtration time increases with GO content, leading to pressure defects in GO film structure since the orderly assembly of GO flakes cannot withstand high-pressure stress. Both aggregates and pressure defects make nonselective paths for passage of gas through the GO membrane and consequently the selectivity decreases (see Fig. 4(a), (c)). However, in this GO content range, carbon dioxide experiences a different trend from other gases. According to Figs. 5 to 8, most changes in the permeance occur at operating pressure of 0.083 to 0.5. The 0.283-15 membrane has the most change among the studied membranes due to the lower kinetic energy of gasses at the low operating pressure [16]. According to Figs. 4(a) to 4(d) and Fig. 7, CO_2 permeance undergoes a different trend from that of N_2 and He at high GO content (0.99 $mgcm^{-2}$ to 1.556 $mgcm^{-2}$). Because CO_2 molecules are more sensitive to functional groups of GO and in this range of GO content, the dominant mechanism for CO_2 transport through the GO membrane is surface diffusion mechanism as opposed to He and N_2. Fig. 14 demonstrates He/CO_2 selectivity and N_2/CO_2 selectivity of the GO membrane synthesized at 10 bar. In the range of 0.00265 $mgcm^{-2}$ to 0.9903 $mgcm^{-2}$, N_2/CO_2 selectivity at operating pressure of 8.3 kPa varies between 1 and 1.2 and CO_2 has the lowest permeance. Kinetic diameters of helium, carbon dioxide, and nitrogen are 2.6, 3.3 and 3.64 Å, respectively [26]. Smaller molecules pass through the membrane more easily; on the other hand, the molecular weight of gas also affects the permeance. According to Knudsen and activated diffusion, which are common mechanisms in the gas separation membranes, the permeance is inversely proportional to the square root of molecular weight. Therefore, N_2/CO_2 selectivity tends to be proportional to $\sqrt{44/28}$ =1.2536. The overall effect of the kinetic diameter and molecular weight of gas molecule causes to the selectivity thus remains in the range of 1 to 1.2. According to Fig. 14, for the membranes synthesized under 10 bar with GO content in the range of 0.9903 to 1.5562 $mgcm^{-2}$, N_2/CO_2 selectivity at operating pressure of 8.3 kPa decreases from 1 to 0.11. The CO_2 permeance of 1.4147 $mgcm^{-2}$-10 and 1.5562 $mgcm^{-2}$-10 membranes is about 9 and 7.7 times more than N_2 permeance and about 1.2 and 3.35 times greater than He one, respectively. This can be verified according to a leading mechanism for each gas. So, carbon dioxide passes through the membrane by a different mechanism in this range of GO content; helium and nitrogen are non-interacting gases, while, carbon dioxide passes through the membrane by interaction with GO functional group and absorption on its surface. Therefore, three parameters that play a significant role in the passage of gas through GO membrane are molecular size, molecular weight, and interaction of penetrating gas with GO functional group.

4. Effect of pH

Fig. 15 shows the effect of pH of GO dispersion on the membrane permeance at various GO content. It reveals that the effect of pH is negligible at low GO content and the optimum value of pH for the GO content of 0.99 $mgcm^{-2}$ is equal to 3.7 (initial pH). The highest permeance occurs at pH=6 due to higher interlayer spacing because of electrostatic repulsion between the layers and the lowest permeance is observed at pH=2 due to lower interlayer spacing because of less electrostatic repulsion and also larger GO nanosheet size which increases tortuosity factor (see section 2.2 in supporting information for detailed information on the effect of pH).

5. Effect of Operating Temperature

Fig. 16 shows the effect of temperature on the permeance of 0.99-10 and 0.0053-10 membranes. The slopes of lines in this figure are activation energy required for gas passage through membrane because the permeance is proportional to $\exp(-ER^{-1}T^{-1})$ [17]. The permeance of 0.0053-10 membrane is more sensitive to temperature than 0.99-10 membrane. Note that the difference in the membrane structure causes a difference in activation energy. The activation energy of 0.99 membrane is more than the 0.0053 one. The lower activation energy of 0.99 membrane can be attributed to the less organized structure of GO membrane at the higher GO content. The resistance of the channels against gas transport is weakened due to the presence of the aggregates in GO film (see section 3.3 and Fig. 11), and then the effective activation energy becomes smaller. Permeance is also a function of the effective pore size, the tortuosity factor, and the membrane thickness. The 0.99

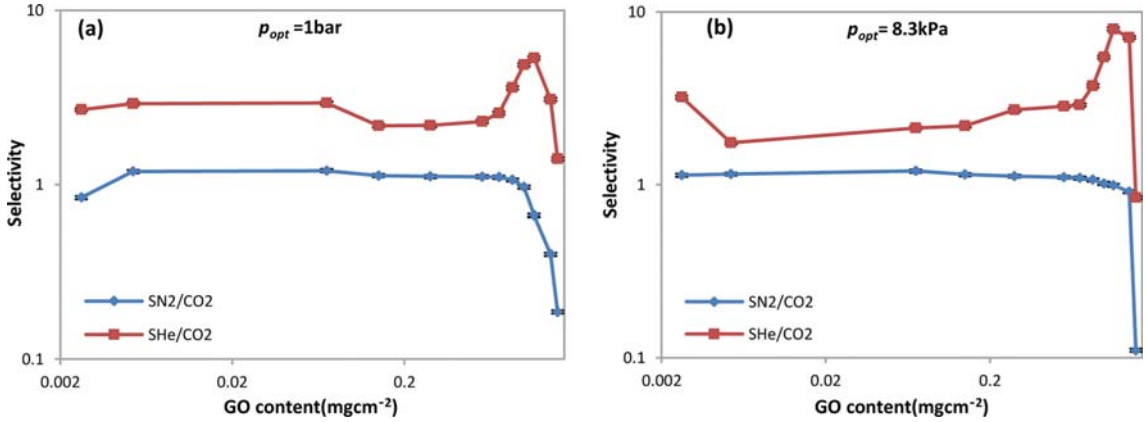

Fig. 14. Selectivity of He/CO_2 and N_2/CO_2 for GO membrane synthesized at 10 bar at various GO contents.

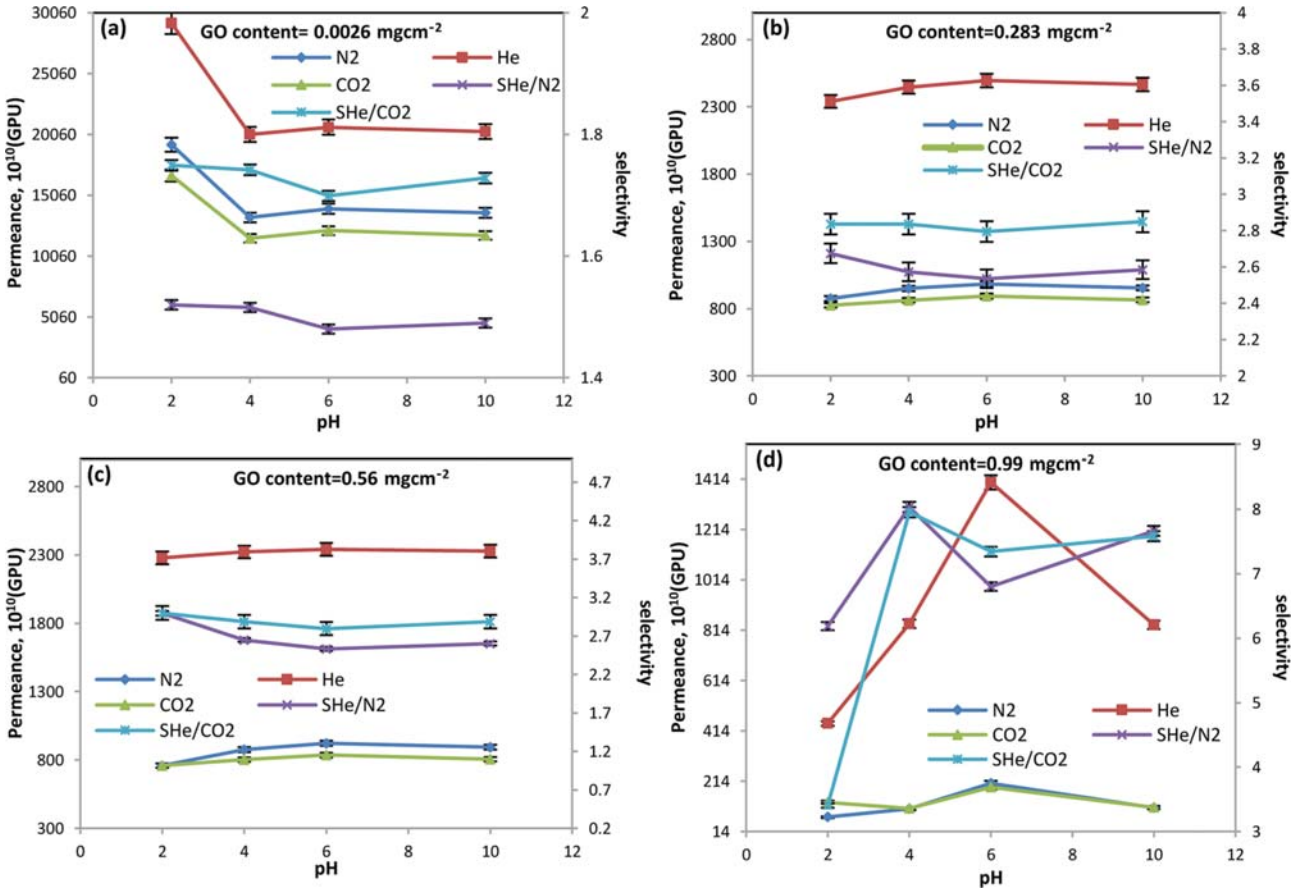

Fig. 15. Effect of pH on permeance and selectivity of GO membrane with p_{syn} of 10 bar and various GO contents.

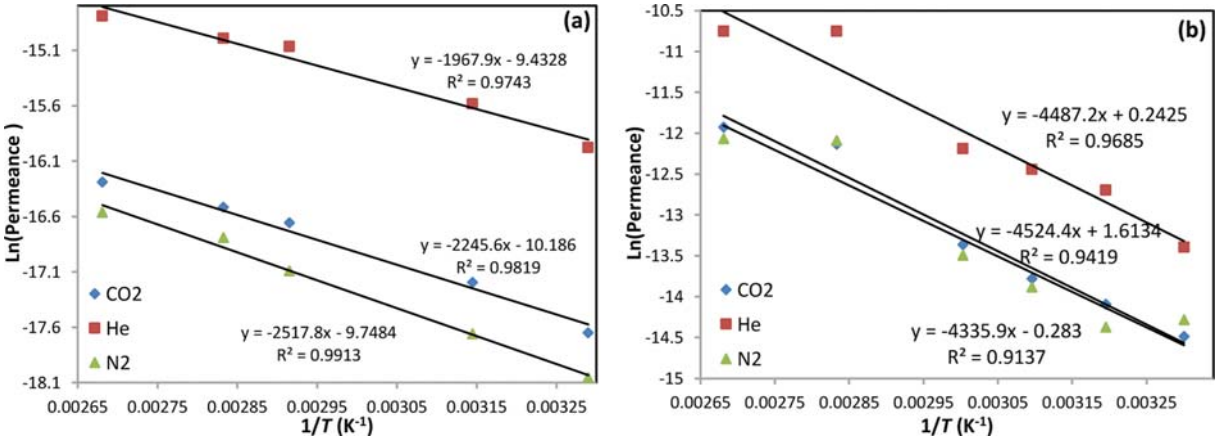

Fig. 16. Effect of temperature on permeance for 0.99-10 membrane (left) and 0.0053-10 membrane (right) at operating pressure of 1 bar.

membrane has a smaller effective diameter, higher the tortuosity factor and higher membrane thickness than the 0.0053 one due to the higher GO content which causes the lower permeance. Finally, these counteracting parameters result in lower permeance in the case of 0.99 membrane.

CONCLUSION

Thin film GO membranes were synthesized by vacuum and pressurized filtration method. GO thin film structure was revealed at a various range of parameters using characterization techniques and gas separation test (He separation from N_2 and CO_2). By tuning various parameters in the synthesis of the substrate, modified ultrafiltration Polyacrylonitrile substrate (12 wt%) was selected as the best substrate among other ultrafiltration and microfiltration substrates (Polyamide membrane, 450 nm). The thickness of GO film is linearly proportional to the GO content during filtration, but the permeance does not hold a linear relationship with GO

content because of pressure defects, interlayer spacing, and aggregates. If filtration is carried out under vacuum or pressures of less than 10 bar, the permeance will decline with operating pressure for all studied GO contents. If the membrane is synthesized under the pressure of 10 bar: the permeance has an ascending-descending trend with operating pressure for GO content in the range of 0.0027 mg/cm^2 to 0.07 mg/cm^2; at very low GO content, the filtration will be finished rapidly and there is not enough time for compression; the gas permeance through thick film GO membrane (1.132 mg/cm^2 to 1.556 mg/cm^2) decreases with operating pressure and upward trend is also seen for moderate GO content. If the synthesis is done under 15 bar filtration: at high GO content (1.1317 mg/cm^2 to 1.55619 mg/cm^2), the permeance is inversely proportional to operating pressure, and at the other GO contents an upward trend will be seen. The undescending trend of the permeance with operating pressure is expected and the reason for declining trend is the aggregates (especially at higher GO content) and insufficient interlayer spacing (especially in the lower synthesis pressure). The optimum value of synthesis pressure in filtration method is equal to 10 bar because it has lower pressure defects compared to pressures greater than 10, and has higher film density compared to pressures less than that. CO_2/N_2 selectivity (CO_2/He selectivity) of 1.41 mgcm^{-2} membrane and 1.556 mgcm^{-2} membrane are 9.06 (1.2) and 7.57 (3.3), respectively; this can be attributed to the dominance of adsorption mechanism to the other ones in CO_2 separation. pH of GO dispersion affects the stability of GO dispersion, functional groups and lateral size of GO flakes. Most permeance occurs at pH=6 due to higher interlayer spacing and the lowest permeance is observed at pH of 2 because of larger GO sheets and lower repulsion force. These findings are useful for a better understanding of many challenges to the GO thin film membrane potential for all separation fields such as desalination, dehydration, and gas separation.

ACKNOWLEDGEMENT

We acknowledge financial support from the Nuclear Science and Technology Research Institute. The authors would like to thank A. Dastbaz for his experimental help and expertise and N. Amini for her assistance in experimental work.

SUPPORTING INFORMATION

Additional information as noted in the text. This information is available via the Internet at http://www.springer.com/chemistry/journal/11814.

REFERENCES

1. H. Ha and E. C. John, *Korean J. Chem. Eng.*, **35**, 1 (2017).
2. X. Li, F. Li and L. Fang, *Korean J. Chem. Eng.*, **32**, 2449 (2015).
3. W. Jia and S. Lu, *Korean J. Chem. Eng.*, **31**, 1265 (2014).
4. T.-D. Nguyen-Phan, V. H. Pham, H. Yun, E. J. Kim, S. H. Hur, J. S. Chung and E. W. Shin, *Korean J. Chem. Eng.*, **28**, 2236 (2011).
5. M. B. Sen and S. Ghosh, *Korean J. Chem. Eng.*, **34**(7), 2079 (2017).
6. W. Gao, M. Majumder, L. B. Alemany, T. N. Narayanan, M. A. Ibarra, B. K. Pradhan and P. M. Ajayan, *ACS Appl. Mater. Interfaces*, **3**, 1821 (2011).
7. W. Choi, J. Choi, J. Bang and J.-H. Lee, *ACS Appl. Mater. Interfaces*, **5**, 12510 (2013).
8. M. Safarpour, A. Khataee and V. Vatanpour, *J. Membr. Sci.*, **489**, 43 (2015).
9. H.-R. Chae, J. Lee, C.-H. Lee, I.-C. Kim and P.-K. Park, *J. Membr. Sci.*, **483**, 128 (2015).
10. R. Nair, H. Wu, P. Jayaram, I. Grigorieva and A. Geim, *Science*, **335**, 442 (2012).
11. R. Joshi, P. Carbone, F. Wang, V. Kravets, Y. Su, I. Grigorieva, H. Wu, A. Geim and R. Nair, *Science*, **343**, 752 (2014).
12. B. Vatsha, J. C. Ngila and R. Moutloali, *J. Membr. Sep. Technol.*, **4**, 98 (2015).
13. Z. P. Smith and B. D. Freeman, *Angewandte Chemie International Ed.*, **53**, 10286 (2014).
14. M. Moochani, A. Moghadassi, S. M. Hosseini, E. Bagheripour and F. Parvizian, *Korean J. Chem. Eng.*, **33**, 2674 (2016).
15. Y. P. Tang, D. R. Paul and T. S. Chung, *J. Membr. Sci.*, **458**, 199 (2014).
16. H. W. Kim, H. W. Yoon, S.-M. Yoon, B. M. Yoo, B. K. Ahn, Y. H. Cho, H. J. Shin, H. Yang, U. Paik and S. Kwon, *Science*, **342**, 91 (2013).
17. H. Li, Z. Song, X. Zhang, Y. Huang, S. Li, Y. Mao, H. J. Ploehn, Y. Bao and M. Yu, *Science*, **342**, 95 (2013).
18. P. Sun, M. Zhu, K. Wang, M. Zhong, J. Wei, D. Wu, Z. Xu and H. Zhu, *ACS Nano*, **7**, 428 (2012).
19. X. Zhao, Y. Su, Y. Liu, Y. Li and Z. Jiang, *ACS Appl. Mater. Interfaces*, **8**, 8247 (2016).
20. J. Wang, P. Zhang, B. Liang, Y. Liu, T. Xu, L. Wang, B. Cao and K. Pan, *ACS Appl. Mater. Interfaces*, **8**, 6211 (2016).
21. P. Sun, K. Wang and H. Zhu, *Adv. Mater.*, **28**, 2287 (2016).
22. G. Liu, W. Jin and N. Xu, *Angewandte Chemie International Ed.*, **55**, 13384 (2016).
23. L. J. Cote, F. Kim and J. Huang, *J. Am. Chem. Soc.*, **131**, 1043 (2008).
24. M. Mulder, *Basic principle of membrane technology*, 2nd Ed., Kluwer Academic (1997).
25. Y. P. Yampol'skii and B. Freeman, *Membrane gas separation*, Wiley Online Library, 34 (2010).
26. E. Albrecht, G. Baum, T. Bellunato, A. Bressan, S. Dalla Torre, C. D'ambrosio, M. Davenport, M. Dragicevic, S. D. Pinto and P. Fauland, *Nuclear Instruments and Methods in Physics Research Section A: Accelerators, Spectrometers, Detectors and Associated Equipment*, **510**, 262 (2003).

Supporting Information

Thin film graphene oxide membrane: Challenges and gas separation potential

Fateme Abbasi*, Javad Karimi-Sabet,†, Cyrus Ghotbi*, and Zeinab Abbasi***

*Department of Petroleum and Chemical Engineering, Sharif University of Technology, Tehran, Iran
**Material and Nuclear Fuel Research School, Nuclear Science and Technology Research Institute, Tehran, Iran
(*Received 15 August 2017 • accepted 4 December 2017*)

EXPERIMENTAL SECTION

1. Materials

Graphite powders, sulfuric acid (95-97%), phosphoric acid, hydrochloric acid (37%), N-methyle-2-pyrrodine, potassium persulfate, phosphorus pentoxide, hydrogen peroxide (30%), potassium permanganate, ethanol, sodium hydroxide were purchased from Merck Company. Polyacrylonitrile was purchased from Isfahan Polyacryl Company. Polyamide membrane (Whatman, 450 nm) was purchased from Aldrich company.

2. Substrate Preparation

Polyacrylonitrile substrate is synthesized by phase inversion method in the optimum condition as follows: PAN powder is dried in an oven at 70 °C then dissolved in N-methyl-2-pyrolidene (NMP) at room temperature for 24 hr to form a 10, 12, 13, 15, 16, 17, 19, and 21 wt% homogeneous solution. After removing air bubbles, these solutions were cast onto nonwoven polyester by motorized machine with uniform speed. The gap of the casting knife was adjusted on 350 μm. Subsequently, they were plunged into the 19 °C water bath, for at least 24 h to remove the solvent. The prepared substrates were dried in the oven at 50 °C, after placed in the room temperature and heated in the NaOH solution (2 M) at 50 °C for 90 min, then immersed into an HCl solution (2 M) at the room temperature for 30 min and after that, the PAN substrates were washed with an excess amount of double distilled water to remove any remaining chemicals impurity.

3. Membrane Preparation

Graphite oxide (G-O) was prepared by the improved Hummers method [1]. The graphite oxide (G-O) was dispersed in dionized water (0.3 $mgml^{-1}$) using an ultrasonicator. The concentrations of 0.2, 0.1, 0.05, 0.025, 0.0125, 0.00625 and 0/.003125 are prepared from an initial graphene oxide (GO) dispersion and their absorption is measured using UV-visible absorption spectra at various wavelengths. 0.3 $mgml^{-1}$ GO dispersion is Centrifuged at 8,000 rpm for several times. This process continues until the concentration after two consecutive centrifugation remains unchanged; after 120 minutes, the absorption of GO dispersion would be measured at a wavelength of 230, 260, 360 and 632 which are equal to 2.96, 2.28, 0.85 and 0.046, respectively. These values remain unchanged for longer centrifugation times. According to Fig. S1, it can be found that GO concentration is approximately equal to 0.14, in other words, the concentration has dropped about 53.3 percent. This homogeneous GO aqueous dispersion is stable more than 9 months. The initial PH of stable colloid is 3.74 which can be tuned using HCl and NaOH at pH of 2, 6 and 10.

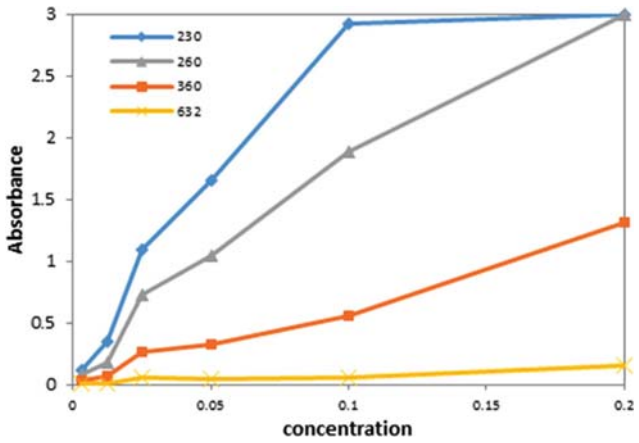

Fig. S1. The absorbance of the prepared standard GO dispersion at various wavelengths.

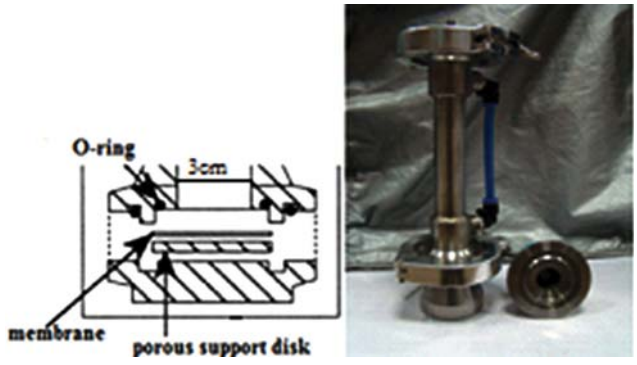

Fig. S2. Image of filtration module (right image) and schematic of bottom part of it(left image). The effective area of the module is $\pi(3^2/4)$ cm^2.

3-1. Filtration Method

Polyacrylonitrile substrate is prepared by phase inversion method. GO dispersions at various concentrations were prepared and 75 ml of them were loaded in the static cell (Fig. S2) and filtered by the 12 wt% modified Polyacrylonitrile ultrafiltration (12mPAN) substrate under vacuum and feed pressures of 2, 6, 10 and 15 bar. After filtration, the thin film GO membrane was slowly dried in a

closed chamber. Gas separation test is performed after drying of GO membrane in the environment and oven at 70 °C for at least 24 hr and vacuum desiccators for removing water completely. To evaluate the effects of microfiltration substrates, commercial polyamide microfiltration membrane with an average pore size of 450 nm was used as the microfiltration substrate.

3-2. Spin Coating and Drop Casting

1 ml of 0.1 $mgml^{-1}$ GO dispersion was dropped at the center of the mPAN substrate (2×3 cm^2) during spun at 3,000 rpm for 1 minute. These steps were also repeated several times (1-20). To synthesize GO membrane by drop casting method, a few drops of GO dispersion were dropped on the mPAN substrate and dried. This process was repeated several times to increase the thickness of GO membrane.

4. Characterization

The crystal structure of the GO powder was characterized by X-ray diffraction (Equinox 3000). The chemical bonds of graphite oxide powder were measured by Fourier Transform Infrared Spectroscopy in the range of 400-4,000 cm^{-1}. To prepare samples for AFM imaging, 0.05 mg/mL GO dispersion was first diluted 14 times and then one drop of it was deposited onto freshly cleaved quartz sheet and dried at room temperature. Surface morphologies of GO sheets were observed using atomic force microscopy under tapping mode (AFM, Veeco, noncontact (NC-AFM) mode, NCHR Si cantilevers). The surface and cross-section morphologies of the substrate and GO thin film membranes were characterized by scanning electron microscopy (AIS 2300 C, Seron Co., Korea) and field emission scanning electron microscope (FESEM, HITACHI S-4160).

5. Gas Permeation Test

Pure gas permeation measurements of GO membranes were performed using a constant-volume variable pressure method at a certain feed pressure and temperature for gas molecules with different kinetic diameters (e.g., He (0.260 nm), N_2 (0.364 nm) and CO_2 (0.330 nm). The permeance was calculated by:

$$Q = \frac{V}{RTA\Delta p}\frac{dp}{dt}\frac{1}{3.35} \quad (S1)$$

where Q, dp/dt, V, ΔP, T, A are the permeance represented in GPU; the rate of the downstream pressure rise under steady state conditions (Pas^{-1}); the downstream volume (m^3); the pressure difference between the two sides (Pa); the measurement temperature (K); the effective area of the membrane in gas separation module (m^2), respectively. All gas permeation tests were performed three times. Run to run sample reproducibility and sample-to-sample reproducibility were high and relative errors from the mean values of permeance were within ±1% and ±5%, respectively. The effective membrane diameter in gas separation module and downstream volume were 1cm and 15 lit or 0.134 lit (depending on the value of membrane permeance), respectively. The ideal separation factor (selectivity) of components 1 and 2 is defined as the ratio of the pure gas permeance of each component:

$$S = \frac{Pe_1}{Pe_2} \quad (S2)$$

The membrane module is heated by heating tape and the temperature is controlled by temperature controller with the accuracy of ±1 °C and ±2 °C for temperature in the range of 40-60 °C and 70-100 °C, respectively.

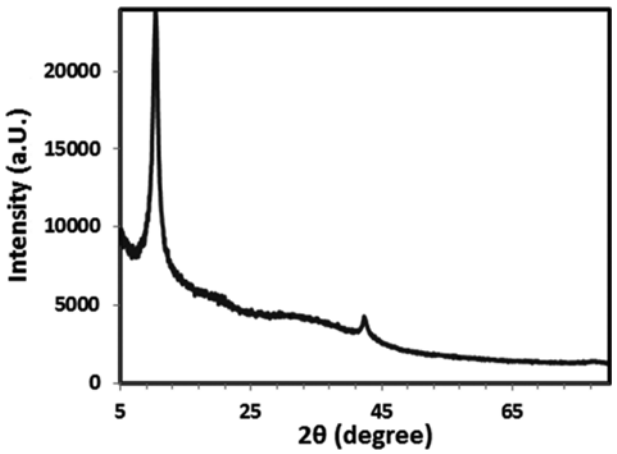

Fig. S3. XRD spectrum of graphite oxide.

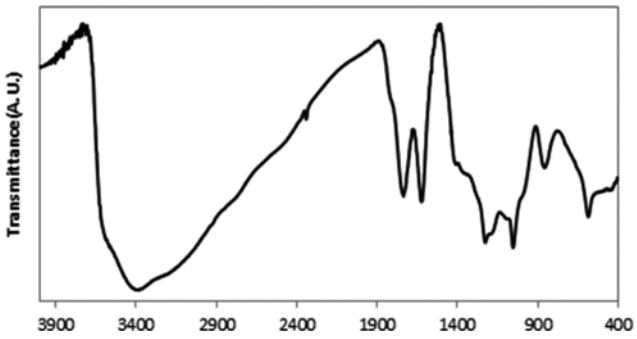

Fig. S4. FTIR spectrum of GO nanosheet.

SUPPORTING NOTES

1. Characterization of Graphite Oxide

XRD pattern was analyzed to understand the phase structure of graphite oxide (G-O). G-O powder shows a characteristic peak at 10.35° corresponding to a d-spacing of 8.54 Å (Fig. S3). The FTIR spectrum in Fig. S4 indicates the presence of hydroxyl, epoxy/ether, and carboxyl groups. These functional groups result in hydrophilicity, hydrogen-bonding interactions between GO nanosheets and proper intersheet spacing that causes the film structural stability and good mechanical strength. The hydrophilicity was reflected by the contact angle, which is shown in Fig. 3. Atomic force microscopy demonstrates the flaky structure and topographical features of exfoliated GO sheets. The thickness (0.9 nm) and the lateral size (423 nm) of GO nanosheets can be clearly seen in the depth profile of Fig. S5. More details of these characterizations have been reported in our previous work [2].

2. Effect of pH on GO Nanosheet

Size and surface chemistry of GO sheets and GO dispersion stability are drastically influenced by pH. The reduction and protonation (deprotonation) of the carboxyl groups on the GO sheets

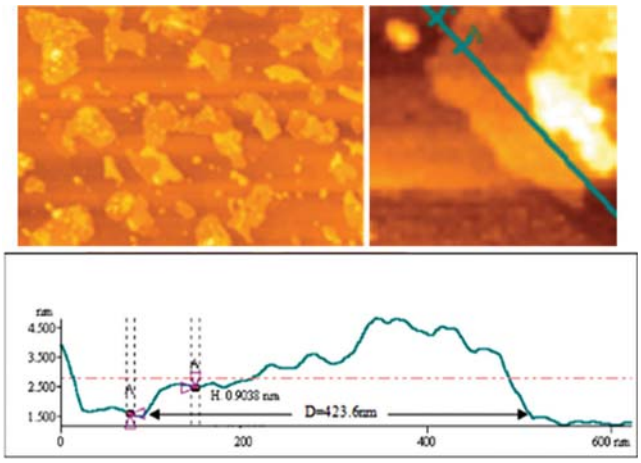

Fig. S5. AFM image of a GO flake.

are responsible for the variation in the surface charge and lateral size of GO. Repulsion between the negatively charged sheets increases in the natural and alkaline environment and is proportional to the surface charge. In an acidic environment, protonation of carboxyl groups reduces the negative charge on the sheets, thereby decreasing electrostatic repulsion between them, which leads to the agglomeration of the sheets at pH less than 2. GO dispersions are stable at the pH range of 4-11, and unstable at both extremes of the pH (2 and 12) due to increase in attractive forces and decrease in the repulsive ones which are originated from protonation or reduction of carboxyl groups. The reader is referred to our previous work [2] for more details on the effect of pH.

3. Selection of the Best Substrate

The aim of this study is to synthesize a thin film graphene oxide for gas separation. Because of low mechanical strength, a suitable substrate is required. In addition, the substrate material and its characteristics are also very important. A suitable substrate should have hydrophilic functional groups on its surface, low surface roughness, good mechanical strength, low resistance against the passage of gas during gas separation test, low resistance to the passage of water during filtration, narrower pore size distribution and the appropriate surface pore size which should be in the range of the ultrafiltration membrane pore sizes. The Polyacrylonitrile (PAN) has been selected as the best polymer for this purpose because it satisfies all mentioned features of the desired substrate. Polymer concentration, the initial evaporation time, bath temperature, solvent and anti-solvent of PAN are effective factors in the synthesis of Polyacrylonitrile substrate. The modification time and temperature of PAN substrate are also two factors that are involved in the modified substrates. Fig. S6 indicates the effect of concentration on the surface of GO/PAN membrane. With increasing polymer concentration, the passage of water through the membrane takes longer, and to achieve uniform surface high driving force is required and thereby a non-uniform surface is observed; therefore, the optimum value for polymer weight fraction is equal to 12 wt%.

The PAN substrate has an asymmetric structure with a top dense skin layer and supporting layer with fingerlike macropores of 77 μm thickness as shown in Fig. S7. Fig. S8 shows the AFM image of 12% modified Polyacrylonitrile ultrafiltration (12mPAN) substrate with average surface roughness of ~6.5 nm.

Substrate modification improved the membrane roughness and hydrophilicity because the -CN groups of PAN were transformed into -COOH groups during the hydrolysis, and $CONH_2$ or -CONH groups were also formed as possible byproducts [3] and theses two factors facilitate the spread of aqueous GO dispersion over the substrate surface. The hydrophilicity was realized by the contact angle,

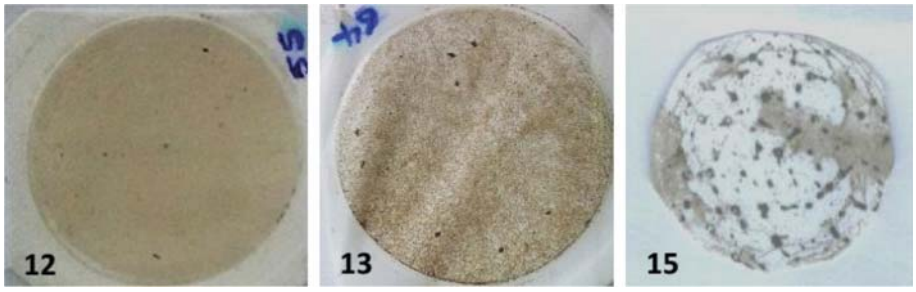

Fig. S6. Effect of concentration of PAN solution on the surface of GO/PAN membrane.

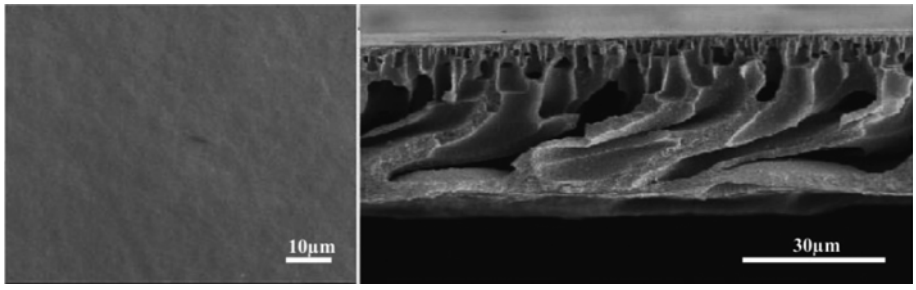

Fig. S7. SEM image of 12%mPAN surface (left image) and FESEM image of cross section of 12%mPAN membrane (right image).

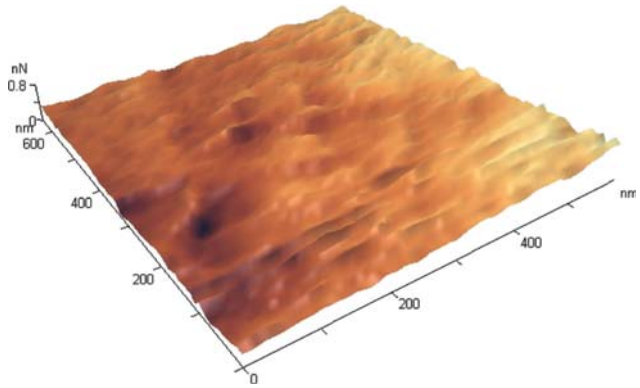

Fig. S8. AFM image of 12% modified Polyacrylonitrile ultrafiltration (12mPAN) substrate.

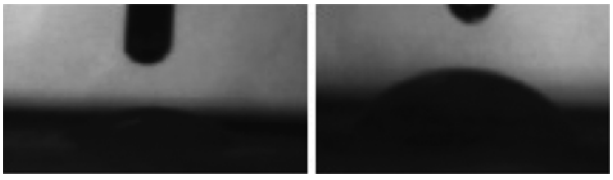

Fig. S9. Contact angle of 12% PAN ultrafiltration substrate before modification (right image. θ=54°) and after that (left image, θ=28°).

as depicted in Fig. S9. Hydrogen bonds can be formed between GO film and substrate during filtration because of -COOH group on the substrate surface. The SEM and FESEM analysis of substrate are shown in Fig. S7.

4. Mean Pore Size and Roughness of Polyamide and 12mPAN

Mean pore size of polyamide membrane has been reported 450 nm by the Whatman company. No pore is observed from the SEM images of 12mPAN so the mean pore size is estimated by AFM image and image J software and is equal to ~30 nm. Fig. S10 shows the AFM images of GO membranes synthesized at 10 bar pressure and various GO content. Average roughness of these membranes are reported in Table S1.

Table S1. Average surface roughness of GO membrane synthesized at 10 bar pressure and various GO content

GO content (mg/cm^2)	Average surface roughness (nm)
0.028	12
0.07	16
0.13	37
0.14	41
0.28	63
0.70	70
0.848	77
1.56	154

5. Effect of Operating Pressure on the GO Membrane Structure

It should be noted that the GO membrane undergoes a physical change in structure with changing synthesis pressure through film density and pressure defects; consequently, this directly affects the membrane performance. Membrane structure is changed with operating pressure but this effect doesn't remain after removing pressure. In other words, with reduction of operating pressure, the arrangement of GO flakes goes back to its previous state. For example, when the operating pressure increases from 8.3 kPa to 1 bar, the membrane permeance decrease due to increase in film density. If the experiment is repeated in the pressure of 8.3 kPa, no reduction in the permeance is observed because the film density has been returned to its previous value (i.e. the value before applying operating pressure of 1 bar).

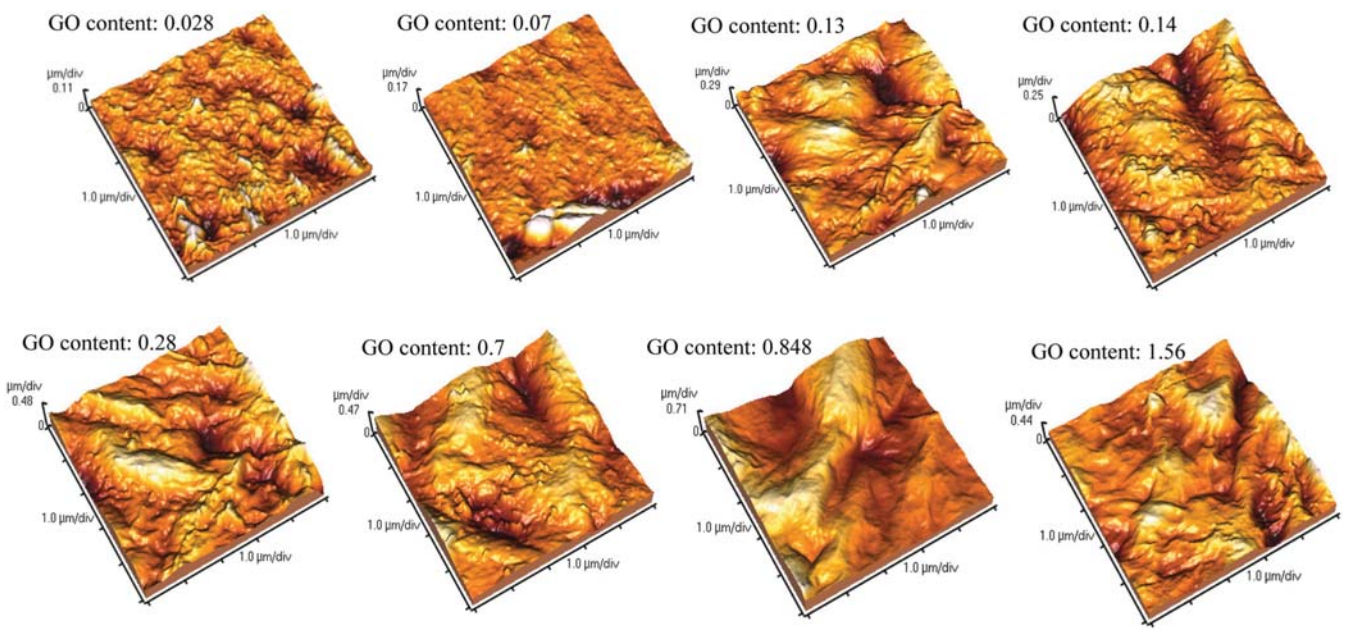

Fig. S10. AFM images of GO membrane synthesized at 10 bar and various GO content.

REFERENCES

1. D. C. Marcano, D. V. Kosynkin, J. M. Berlin, A. Sinitskii, Z. Sun, A. Slesarev, L. B. Alemany, W. Lu and J. M. Tour, *ACS Nano*, **4**, 4806 (2010).
2. F. Abbasi, Z. Abbasi, J. K. Sabet, C. Ghotbi, S. A. Mousavi and N. Amini, *Scientia Nanotechnology*, **24**, 3554 (2016).
3. N. W. Oh, J. Jegal and K. H. Lee, *J. Appl. Polym. Sci.*, **80**, 2729 (2001).